

Towards tailored magnetic anisotropy: A first-principles study of L1₀ FeNi ultrathin films

Joanna Marciniak and Mirosław Werwiński*
Institute of Molecular Physics, Polish Academy of Sciences,
M. Smoluchowskiego 17, 60-179 Poznań, Poland
(Dated: April 5, 2024)

In previous experiments, thin films of L1₀ FeNi with different surfaces, including (001), (110) and (111), were produced and studied. Each surface defines a different alignment of the crystallographic tetragonal axis with respect to the film's plane, resulting in different magnetic anisotropies. In this study, we use density functional theory calculations to examine three series of L1₀ FeNi films with surfaces (001), (010), and (111), and with thicknesses ranging from 0.5 to 3 nm (from 4 to 16 atomic monolayers). Our results show that films (001) have perpendicular magnetic anisotropy, while (010) favor in-plane magnetization, with a clear preference for the tetragonal axis [001]. We propose calling this type of in-plane anisotropy *fixed in plane*. A film with surface (111) and a thickness of four atomic monolayers has the magnetization easy axis almost perpendicular to the plane of the film. As the thickness of the (111) film increases, the direction of magnetization rotates towards a tetragonal axis [001], positioned at an angle of about 45° to the plane of the film. Furthermore, the magnetic moment of ultrathin films increases by a maximum of 5%, and the most significant changes in spin and orbital magnetic moments occur at a depth of about three near-surface atomic monolayers. The presented results could be useful for experimental efforts to synthesize ultrathin L1₀ FeNi films with different surfaces. Ultrathin L1₀ FeNi films with varying magnetic anisotropies may find applications in spintronic devices.

I. INTRODUCTION

The ordered L1₀ FeNi was first discovered in neutron bombarded specimens [1–3] and later identified in samples cut from meteorites [4, 5]. However, the body-centered tetragonal L1₀ structure was found earlier in other binary compounds, such as CoPt and FePt [6]. The name *tetrataenite* of L1₀ FeNi is related to its tetragonal structure and the term *taenite* used for Fe-Ni fcc phase [7]. Studies of natural L1₀ FeNi samples from various meteorites [4, 5, 8–12] are being conducted in parallel with research on ordered FeNi thin films produced in laboratories. Takanashi, co-author of numerous papers on L1₀ FeNi thin films [13–29], summarized investigations of ordered FeNi thin films in a 2017 topical review [30]. The study of Takanashi *et al.* was complemented by other experimental groups [31–36]. Mandal *et al.* concluded the experimental characteristics of bulk and thin-film L1₀ FeNi in a 2023 review article [37].

Measurements of L1₀ FeNi films with thickness less than 5 nm [38, 39] give an important context for the calculation results we present in this work. Kojima *et al.* [39] have presented the dependence of order parameter, magnetization, and magnetic anisotropy on the number of monolayers. For thicknesses of about 10 atomic monolayers (~1.5 nm), low values of both the order parameter and the uniaxial magnetic anisotropy constant were observed [39].

The magnetic properties of the L1₀ FeNi phase are as follows: Curie temperature of about 830 K [11], magnetic moment of about 1.7 μ_B atom⁻¹ [34], upper limit of magnetocrystalline anisotropy constants (K_1)

of 1.3 MJ m⁻³ [3, 40], and room-temperature coercivity (H_c) of 95.5 kA m⁻¹ (1.2 kOe) [11]. The transformation of FeNi from an ordered to a disordered phase occurs at a temperature of 593 K (320°C) [40, 41]. Whereas, obtaining samples with high values of the long-range order parameter (S) is difficult [30]. For L1₀ FeNi (001) films with a thickness of 50 × (Fe atomic monolayer / Ni atomic monolayer), the highest observed value of S is 0.48 [30]. The uniaxial magnetic anisotropy constant (K_u) depends on S [30], and S equal to 0.48 corresponds to K_u of 0.7 MJ m⁻³ (7.0 × 10⁶ erg cm⁻³) [30]. Since this value of K_u is smaller than the shape anisotropy ($2\pi M_s^2$) estimated for FeNi films as 0.9 MJ m⁻³ (9.0 × 10⁶ erg cm⁻³), it has not been possible to manufacture FeNi (001) films with a perpendicular magnetic anisotropy so far [30]. However, Takanashi *et al.* estimated that increasing the order parameter S above 0.7 should raise the K_u above the shape anisotropy value [30].

The properties of the L1₀ FeNi bulk phase were also investigated using density functional theory (DFT) [11, 42–55]. The computational method has been used to determine, among others, the magnetocrystalline anisotropy energy (MAE) of a perfect L1₀ FeNi crystal [42–45, 47], to study the effect of chemical disorder [48, 52–54], and to predict how different substitutions affect the MAE [46, 50, 51].

Despite extensive experimental work on L1₀ FeNi thin films and numerous computational studies on L1₀ FeNi bulk, L1₀ FeNi magnetic thin films have not been modeled from first principles. Only the adsorption of ethylene (C₂H₄) [56] and hydrazine (N₂H₄) [57] on the L1₀ FeNi (111) surface were calculated from DFT. However, magnetic L1₀ thin films were studied with DFT for other L1₀ phases, such as FePt, CoPt, and MnGa [58–63]. In this work, we study ultrathin L1₀ FeNi films, continuing our DFT investigation of L1₀ phases [47, 63, 64],

* Corresponding author: werwinski@ifmpan.poznan.pl

After discussing bulk and thin films, the third form of the $L1_0$ FeNi phase are nanoparticles with the average particle size of a few tens of nanometers [65, 66]. As for thin films, no DFT calculations have been performed so far for $L1_0$ FeNi nanoparticles. Although this would be possible, as shown, for example, in work on $L1_0$ PtZn, PtCo, and Pt(Ni/Co) nanoparticles [67–69]. However, the $L1_0$ FeNi nanostructure was investigated using micro-magnetic simulations, and the effect of the shape of the nanoparticle on the maximum energy product (BH_{\max}) was determined [70, 71].

Although considerable progress has been made in the production of bulk $L1_0$ FeNi phase [72–74], practical applications of this material are yet to come. Noteworthy are the low price of FeNi constituent elements and the high value of its magnetic anisotropy constant at room temperature. Relatively good semi-hard magnetic properties suggest that $L1_0$ FeNi may find use as a permanent magnet that does not contain rare-earth elements [37, 75–77]. Moreover, atomic-scale layering implies the possibility of using $L1_0$ FeNi thin films in spintronic devices [30, 62]. Practical applications for ordered $L1_0$ FeNi nanoparticles are also expected [65, 66].

In this work, the first-principles calculate were made for ultrathin $L1_0$ FeNi films with surfaces (001), (010) and (111). The study aims to determine the films’ magnetic moments and magnetic anisotropies. Answering the question of how they depend on the thickness and type of surface can help obtain FeNi films with different types of magnetic anisotropy, such as perpendicular, tilted, or fixed in-plane. Although perpendicular magnetic anisotropy is fairly well known, it is worth briefly discussing the other two types.

In 2005, a system with the magnetization direction tilted from the plane of the film was prepared experimentally, and it was shown that deflecting it to 45° minimizes the value of the switching magnetic field [78, 79]. Since the magnetization direction of $L1_0$ crystals agrees with the tetragonal axis, a natural candidate for systems with tilted anisotropy are $L1_0$ (111) films. Previous experiments on the $L1_0$ FePt (111) films showed that the direction of magnetization is tilted by $33\text{--}36^\circ$ from the plane of the film, i.e., it points roughly in the direction of the tetragonal axis [80]. In our computational work on FePt ultrathin films, we also dealt with this issue [63]. Here, we will determine the magnetization angle for $L1_0$ FeNi (111) films.

Just as the tetragonal axis alignment leads to perpendicular magnetic anisotropy in films (001) and tilted magnetic anisotropy in films (111), in films (010), it results in an unconventional type of in-plane anisotropy that has a preferred direction in the film plane. We already postulated that such a uniaxial configuration could be called *fixed in-plane* magnetic anisotropy, as opposed to conventional *in-plane* [63]. 20 nm $L1_0$ FeNi (110) films with a tetragonal axis in the plane of the film were experimentally obtained in 2023 and showed order parameter S of 0.6 and magnetic anisotropy constant of 0.55 MJ m^{-3} [28]. Experimental work on isostructural

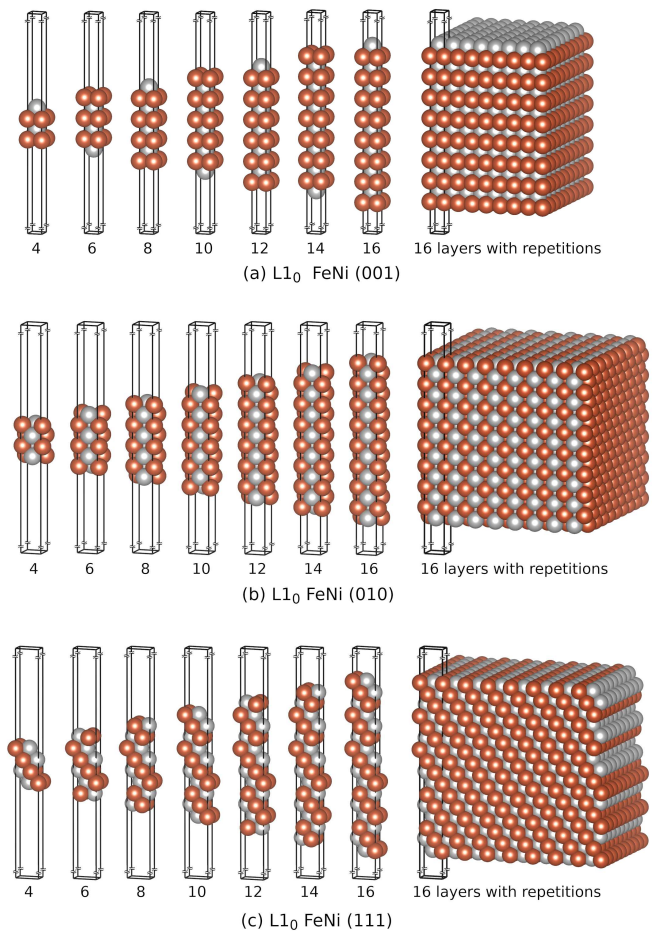


FIG. 1. Unit cell series of $L1_0$ FeNi thin films with (001), (010), and (111) surfaces and thickness from 4 to 16 atomic monolayers; from 0.5 to 2.7 nm for (001) and (010) films and from 0.6 to 3.1 nm for (111) films. On the right, 16-monolayer unit cells were repeated several times in two directions in the plane of the film to visualize the layered character of the models. The vacuum height (at least 30 \AA) has been reduced in the figures to save space.

$L1_0$ FePt (010) films are also known [81–85]. In this work, we will determine the magnetic easy axis of $L1_0$ FeNi (010) films.

II. CALCULATIONS’ DETAILS

We prepared models of $L1_0$ FeNi (001), (010), and (111) thin films in the thickness range from four to sixteen atomic monolayers, see Fig. 1. To keep the concentration of Fe and Ni equal, we considered only films with an even number of monolayers. As a starting point for modeling thin films, we used a unit cell of the $L1_0$ FeNi bulk phase (s.g. $P4/mmm$, $a' = 3.56/\sqrt{2} \sim 2.52$ and $c = 3.58 \text{ \AA}$) [47]. We added a minimum of 30 \AA vacuum to all unit cells of the thin films in the direction perpendicular to the film plane.

For the prepared models, calculations were performed using the full-potential local-orbital (FPLO18.00-52)

TABLE I. Structural data of L1₀ FeNi (001), (010), and (111) thin films consisting of 16 atomic monolayers. The c parameters of the computational unit cells include a vacuum of at least 30 Å. The thicknesses (without vacuum) of the considered (001), (010), and (111) films are 27, 27, and 31 Å, respectively. Unit cell parameters (a , b , c) are given in Å.

| Atom | (001) | | | (010) | | | (111) | | |
|------|-------------|-------|--------|-------------|------|-------|---------------|--------|--------|
| | s.g. $P4mm$ | | | s.g. $Pmma$ | | | s.g. $P12/m1$ | | |
| | a | b | c | a | b | c | a | b | c |
| | 2.52 | 2.52 | 56.85 | 3.56 | 3.58 | 56.70 | 2.52 | 4.38 | 60.89 |
| Fe | 0.00 | 0.00 | -0.484 | -0.25 | 0.00 | 0.484 | 0.00 | 0.335 | -0.483 |
| Ni | 0.50 | -0.50 | 0.484 | 0.25 | 0.50 | 0.484 | 0.50 | -0.165 | -0.483 |
| Fe | 0.00 | 0.00 | 0.453 | 0.25 | 0.00 | 0.453 | 0.00 | 0.004 | -0.449 |
| Ni | 0.50 | 0.50 | -0.453 | -0.25 | 0.50 | 0.453 | -0.50 | -0.496 | -0.449 |
| Fe | 0.00 | 0.00 | -0.422 | -0.25 | 0.00 | 0.422 | 0.00 | -0.327 | -0.416 |
| Ni | 0.50 | 0.50 | 0.422 | 0.25 | 0.50 | 0.422 | -0.50 | 0.173 | -0.416 |
| Fe | 0.00 | 0.00 | 0.390 | 0.25 | 0.00 | 0.391 | 0.00 | 0.343 | -0.382 |
| Ni | 0.50 | 0.50 | -0.390 | -0.25 | 0.50 | 0.391 | -0.50 | -0.157 | -0.382 |
| Fe | 0.00 | 0.00 | -0.359 | -0.25 | 0.00 | 0.360 | 0.00 | 0.012 | -0.348 |
| Ni | 0.50 | 0.50 | 0.359 | 0.25 | 0.50 | 0.360 | -0.50 | -0.488 | -0.348 |
| Fe | 0.00 | 0.00 | 0.328 | 0.25 | 0.00 | 0.328 | 0.00 | -0.321 | -0.315 |
| Ni | 0.50 | 0.50 | -0.328 | -0.25 | 0.50 | 0.328 | -0.50 | 0.180 | -0.315 |
| Fe | 0.00 | 0.00 | -0.296 | -0.25 | 0.00 | 0.297 | 0.00 | 0.353 | -0.281 |
| Ni | 0.50 | 0.50 | 0.296 | 0.25 | 0.50 | 0.297 | -0.50 | -0.147 | -0.281 |
| Fe | 0.00 | 0.00 | 0.265 | 0.25 | 0.00 | 0.266 | 0.00 | 0.010 | -0.248 |
| Ni | 0.50 | -0.50 | -0.266 | -0.25 | 0.50 | 0.266 | 0.50 | -0.489 | -0.248 |

code [86, 87] within the density functional theory (DFT). The exchange-correlation potential in the Perdew-Burke-Ernzerhof (PBE) form was used [88]. The atomic positions of the films were optimized using forces in a spin-polarized approach, with a convergence criterion of 10^{-3} eV Å⁻¹. Table I shows space groups, calculated Wyckoff positions, and unit cell parameters of the example 16-monolayer films. The prepared (001) and (010) films cover the thickness range from 0.5 to 2.7 nm, while the (111) films span from 0.6 to 3.1 nm (all values determined as the distance between the atomic positions of the surface sites).

The k-mesh was considerably densified in the next step, to determine the accurate magnetocrystalline anisotropy energy (MAE) values. For (001) and (010) films, a k-mesh of $60 \times 60 \times 5$ was assumed, and for (111) films, a k-mesh of $60 \times 30 \times 5$. For Brillouin zone integration, the tetrahedron method was chosen. For scalar-relativistic calculations, a 10^{-6} density convergence criterion was used. After self-consistent scalar-relativistic calculations, one iteration of fully-relativistic calculations was performed for the selected quantization axes. Such fully-relativistic solutions were used to determine magnetic anisotropy energies and energy dependencies as a function of the quantization axis (magnetization) direction. As demonstrated [89], this approach leads to sufficiently accurate results, significantly reducing computation time. Calculations of the energy dependence of the

magnetization direction were performed for 10-monolayer films (010) and (111) using unit cells with space group $P1$. For (111) films, having established that the energy minimum is in the (100) plane, calculations were carried for directions varying in this plane every 2°. The direction of easy magnetization was then determined using third-degree polynomial fitting.

The unique implementation of the fixed spin moment method in a fully-relativistic approach allowed us to determine the dependence of the magnetocrystalline anisotropy energy on the spin magnetic moment. We performed these calculations with the PBE exchange-correlation functional in the generalized gradient approximation (GGA), as well as with the Perdew-Wang (PW92) functional in the local density approximation (LDA) [90].

Because the DFT implementation used in this work is based on the linear combination of atomic orbitals, it was possible to perform population analysis using Mulliken's method [91]. We used the VESTA code to prepare drawings of the structures [92]. We discussed the limitations of the models adopted and the approximations used in our previous article on ultrathin films of L1₀ FePt [63].

III. RESULTS AND DISCUSSION

While much is already known about L1₀ FePt [63] and L1₀ CoPt [93] ultrathin films, systematic research on L1₀ FeNi ultrathin films has yet to be conducted, and we hope this theoretical work can be a signpost in that direction. Although several experimental works have already touched on ultrathin L1₀ FeNi films below 5 nm, the results obtained so far [38, 39] give only a fragmentary picture. In contrast, much is already known about L1₀ FeNi thin films with a thickness of about 100 atomic monolayers (about 18 nm), as such a thickness was favored in experiments of Takanashi *et al.* [13–30]. As in the case of bulk L1₀ FeNi, the researchers also tried to obtain the highest magnetic anisotropy for the L1₀ FeNi thin films. The goal is for the uniaxial magnetic anisotropy to exceed the shape magnetic anisotropy value ($2\pi M_s^2 \sim 0.9$ MJ m⁻³ [39]), which will yield perpendicular magnetic anisotropy in (001) films. However, this is hindered by insufficient ordering of L1₀ structure, which significantly reduces the hypothetical maximum attainable value of uniaxial anisotropy K_u . So far, it has been possible to obtain L1₀ FeNi (001) films with an order parameter S of about 0.5 [39]. Kojima *et al.* predict that K_u will exceed the shape anisotropy only above S around 0.6 [39]. In addition to the lack of complete L1₀ ordering, the films are also not perfectly periodic but contain grains that further negatively affect the magnetic anisotropy. For the L1₀ phase, it is assumed that three basic nanocrystal variants are present in a single sample, and their main crystallographic axes do not necessarily point in the same direction [54].

Although the vast majority of previous work on L1₀ FeNi films has explored a geometry in which alter-

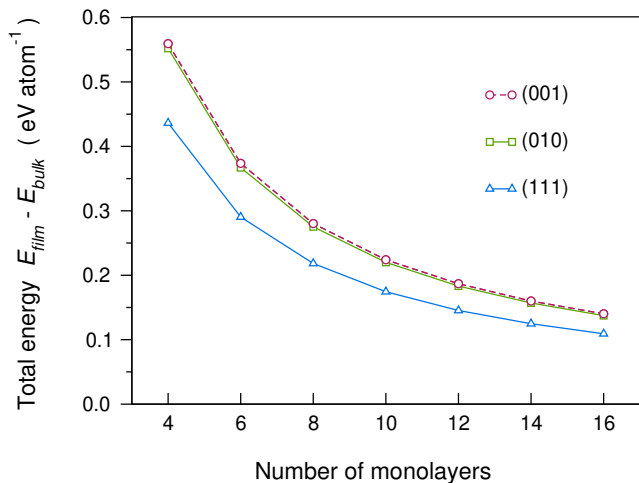


FIG. 2. Differences between film energy and bulk energy, calculated for $L1_0$ FeNi films with (001), (010), and (111) surfaces. Calculations were performed using the FPLO18 code with the PBE exchange-correlation functional.

nating Fe and Ni monolayers are oriented in the plane of the film [surface (001)] [13–30], this is neither the only nor the most energetically favorable possibility. Another type of arrangement of atomic monolayers is an orientation perpendicular to the surface of the film [e.g., surface (110) or equivalent surfaces (010) and (100)]. In 2023, by denitridation of FeNiN(110) films, the 20 nm $L1_0$ FeNi (110) films were obtained and indicated relatively large S of 0.6 and K_u of 0.55 MJ m^{-3} [28]. Also in 2023, 30 nm $L1_0$ FeNi (111) films were produced [36]. Although the order parameter S was not determined for (111) films, Nguyen *et al.* describe them as ordered, which is further suggested by the high K_u value of 1.15 MJ m^{-3} .

Although other surfaces are also possible, this work focuses only on surfaces (001), (010), and (111). Even though the prepared and calculated models allow us to understand numerous properties of layered systems, they have significant limitations, which can only be overcome in a more advanced approach. Namely, the models considered include neither disorder of $L1_0$ structure nor microstructure and describe the films without the substrate or capping layer. However, the lack of a substrate can be simultaneously an advantage, as it allows for the determination of the properties of the FeNi film itself, which would be difficult in the experiment.

III.1. Energetic stability

The total energy of the films decreases with thickness, tending asymptotically to the bulk value, see Fig. 2. Over the considered range, the most energetically stable films are (111), then (010), and last (001), with the energy of the (111) surface being much lower than the other two. Previously, the same order was determined for the surfaces of $L1_0$ FePt and $L1_0$ CoPt films [94]. This result identifies a suboptimal energy condition for (001) surface

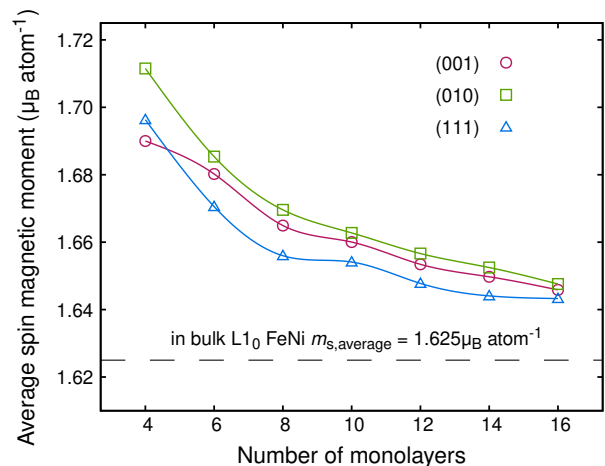


FIG. 3. Averaged spin magnetic moment as a function of the number of atomic monolayers of $L1_0$ FeNi ultrathin films. The dashed horizontal line indicates the corresponding result calculated for bulk $L1_0$ FeNi [47]. The FPLO18 code with the PBE exchange-correlation functional was used for calculations.

formation and a preference for (111) surface. Moreover, a significant increase in total energy per atom with a decrease in the number of monolayers suggests difficulties in obtaining uniform ultrathin films and an energetic preference for forming thicker systems.

III.2. Magnetic moments

In this work, we determined magnetic moments, magnetization directions, and magnetic anisotropy energies of considered films. Figure 3 showing the dependence of the averaged spin magnetic moment on the number of monolayers resembles the total energy plot, see Fig. 2. The values of magnetic moments decrease asymptotically to the values calculated for bulk [47], which is typical behavior for magnetic films. It was observed experimentally for Fe [95] and calculated for FePt [63], for example. The effect originates in elevated magnetic moment values on several (about three in our case) near-surface monolayers. Since our models have two surfaces (top and bottom), it is only above a film thickness of about six atomic monolayers that a central section of the film, with magnetic moments close to bulk value, begins to form. Further growth in thickness increases the contribution from the central region.

Figure 4 presents the spin and orbital magnetic moments on individual atoms along film thickness. We can see the mentioned increase in magnetic moments on about three surface monolayers and values close to the bulk value in the central region [47]. The highest values of spin (and orbital) magnetic moments are on the surface (010), which correlates with the highest average spin moments in Figure 3. Magnetic moments on the surfaces are elevated throughout the thickness range considered; the central region vanishes only below about six mono-

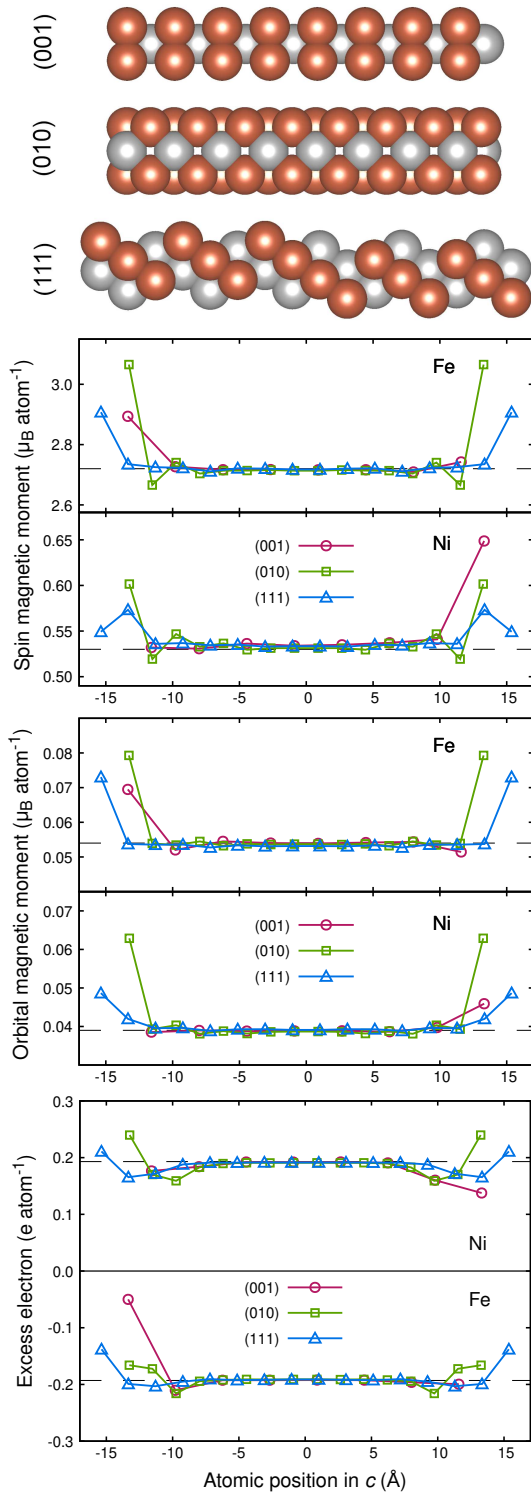


FIG. 4. Spin and orbital magnetic moments and excess electrons in 16-monolayer films of L₁₀ FeNi with surfaces (001), (010), and (111). Dashed lines indicate bulk values: spin magnetic moments on Fe (Ni) equal to $2.72 \mu_B$ ($0.53 \mu_B$), orbital magnetic moments on Fe (Ni) equal to $0.054 \mu_B$ ($0.039 \mu_B$), and excess electron of $\pm 0.193 e$. Calculations were performed using the FPLO18 code with the PBE exchange-correlation potential. Above the charts are the side views of the film unit cells.

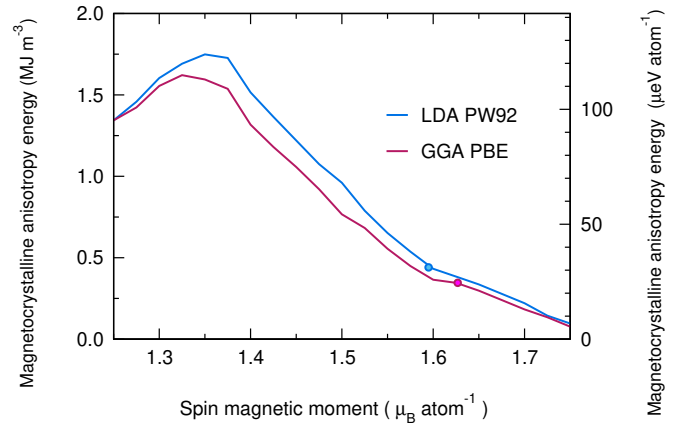


FIG. 5. Magnetocrystalline anisotropy energy of the bulk L₁₀ FeNi as a function of the spin magnetic moment. Calculations were performed using the FPLO18 code with the LDA PW92 and GGA PBE exchange-correlation potentials. Circles represent equilibrium results.

layers. Unlike the (010) and (111), the model of (001) film has asymmetrical *top* and *bottom* surfaces (one side ends in an Fe monolayer and the other in Ni). Hence, the observed asymmetry in the (001) results in Figure 4.

Figure 4 also shows excess electrons on Fe and Ni atoms along the thickness of films, which were calculated using the Mulliken's approach [91]. As is the case for magnetic moments, in the central region of the films the excess electron (hole) values are close to those for bulk FeNi, while for about three surface monolayers they show large deviations from bulk value. We observed similar behavior in the results of additional calculations performed without spin polarization, confirming the primary role of charge transfer in the formation of perturbations in the near-surface monolayers. Furthermore, the deviations in excess electrons on FeNi surfaces (ranging from about -0.02 to 0.15 on Fe sites) are much smaller than those calculated previously for FePt surfaces (ranging from about -1.0 to 1.0 on Fe sites) [63]. This indicates higher stability of FeNi surfaces.

III.3. Magnetic anisotropy

For ultrathin films of L₁₀ FeNi, we observed an increase in the magnetic moment only to about 5% over the bulk value. The magnetic anisotropy of thin films can differ much more. In the case of magnetic anisotropy, we are interested in both the value of the magnetic anisotropy energy and the direction of magnetization relative to the plane of the film (magnetic easy axis). We expect that since the films under consideration have an L₁₀ structure with a unique tetragonal axis, the direction of magnetization will be along or close to this axis. This means that perpendicular, in-plane, and tilted magnetic anisotropy should be observed for the films (001), (010), and (111), respectively.

For bulk L₁₀ FeNi, the MAE of 0.34 MJ m^{-3}

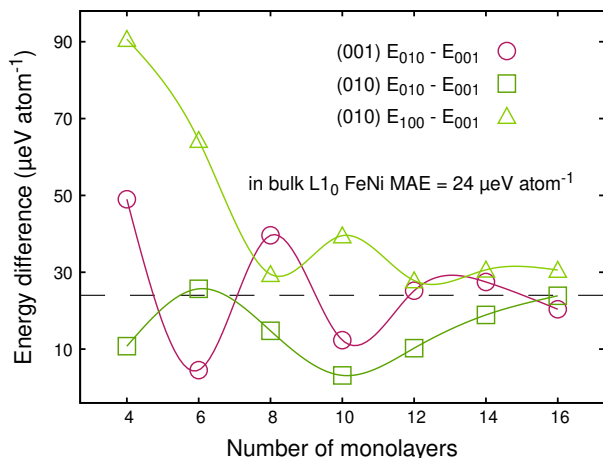


FIG. 6. Magnetic anisotropy energies as a function of the number of atomic monolayers of $L1_0$ FeNi (001) and (010) ultrathin films. The dashed horizontal line indicates the magnetocrystalline anisotropy energy (MAE) calculated for bulk $L1_0$ FeNi ($24 \mu\text{eV atom}^{-1}$) [47]. The energies E_{001} , E_{010} , and E_{100} were determined for the corresponding magnetization directions using the FPLO18 code with the PBE exchange-correlation functional.

($24 \mu\text{eV atom}^{-1}$) determined from the GGA is much lower than the maximum determined values of experimental magnetic anisotropy constants of up to 1.3 MJ m^{-3} [40]. The discrepancy may be due to the temperature for which the DFT calculations are done (by definition, 0 K) or the limitations of the GGA. Furthermore, in our work on bulk $L1_0$ FePt, we pointed out that the values of MAE and magnetic moment are correlated [64], and the latter depends on the choice of the exchange-correlation potential. To show this correlation also for bulk $L1_0$ FeNi, we performed calculations of the dependence of MAE on a fixed spin moment for LDA and GGA functional. Figure 5 shows that for $L1_0$ FeNi the equilibrium values of magnetic moments and magnetocrystalline anisotropy energies obtained in the PW92 and PBE approximations differ only slightly. Moreover, the MAE value depends on the magnetic moment, and in both approximations it has a maximum above 1.5 MJ m^{-3} for a reduced magnetic moment of about $1.35 \mu_B \text{ atom}^{-1}$. The presented relation of MAE and magnetic moment may explain the discrepancy between the experimentally determined K_u values above 1 MJ m^{-3} at room temperature and the calculated MAE values below 0.5 MJ m^{-3} at 0 K. Namely, K_u can also indirectly depend on temperature via temperature-mediated reduction of magnetization. Such interpretation is supported by calculations of the MAE dependence on temperature for $L1_0 \text{ Fe}_{0.56}\text{Ni}_{0.44}$, showing lowered MAE at low temperatures and MAE maximum near room temperature [54]. Furthermore, K_u measurements of $L1_0$ FeNi films performed at 35 K reveal much lower K_u values ($< 0.2 \text{ MJ m}^{-3}$) than typical results obtained at room temperature [33].

We will begin our discussion of the magnetic anisotropy

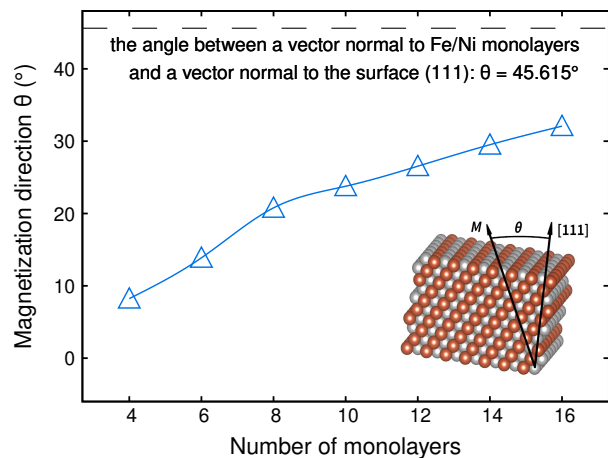


FIG. 7. Magnetization direction as a function of the number of atomic monolayers of $L1_0$ FeNi (111) thin films. The calculations were performed using the FPLO18 code with PBE exchange-correlation potential. The horizontal dashed line indicates the angle value between the vector [001] normal to the plane of the Fe/Ni atomic monolayers and the vector [111] normal to the film's surface.

of $L1_0$ FeNi films with the best-known (001) films. As in the previous experiments [13–30], we also expect for them the perpendicular magnetic anisotropy. The relation of total energy and magnetic moment on the number of monolayers suggest that also for magnetic anisotropy energy we should expect a dependence that converges asymptotically to the bulk value. However, as we can see in Fig. 6, although the anisotropy energy of the (001) films converges to the bulk value, this is accompanied by pronounced oscillations. This type of MAE behavior has been observed in several previous calculations for ultrathin films [58, 63, 96–99]. Oscillations of uniaxial magnetic anisotropy have also been observed experimentally for ultrathin bcc Fe and fcc Co films with periods of 5.9 and 2.3 atomic monolayers, respectively [100]. They are due to quantum well states situated around the Fermi level [100] and come from the quantum size effect appearing in small enough systems. The positive values of the magnetic anisotropy energies for films (001), as defined as $E_{010} - E_{001}$, indicate a preference for orientation of the direction of magnetization perpendicular to the plane of the (001) film. However, the result obtained does not clearly identify perpendicular anisotropy, since for this, the uniaxial anisotropy energy must exceed the energy of shape anisotropy ($2\pi M_s^2 \sim 0.9 \text{ MJ m}^{-3}$ [39]). This criterion is not met in case of our computational results. Nevertheless, uniaxial anisotropy is expected to overcome the shape anisotropy in experiments where the determined K_u value is up to three times higher than the GGA value calculated here.

For films (010) with Fe/Ni monolayers aligned perpendicular to the plane of the film (*bookshelf* arrangement), we expect an axis of easy magnetization in the direction of the crystallographic tetragonal axis, that is, in the plane of the film. Indeed, this direction of magnetization

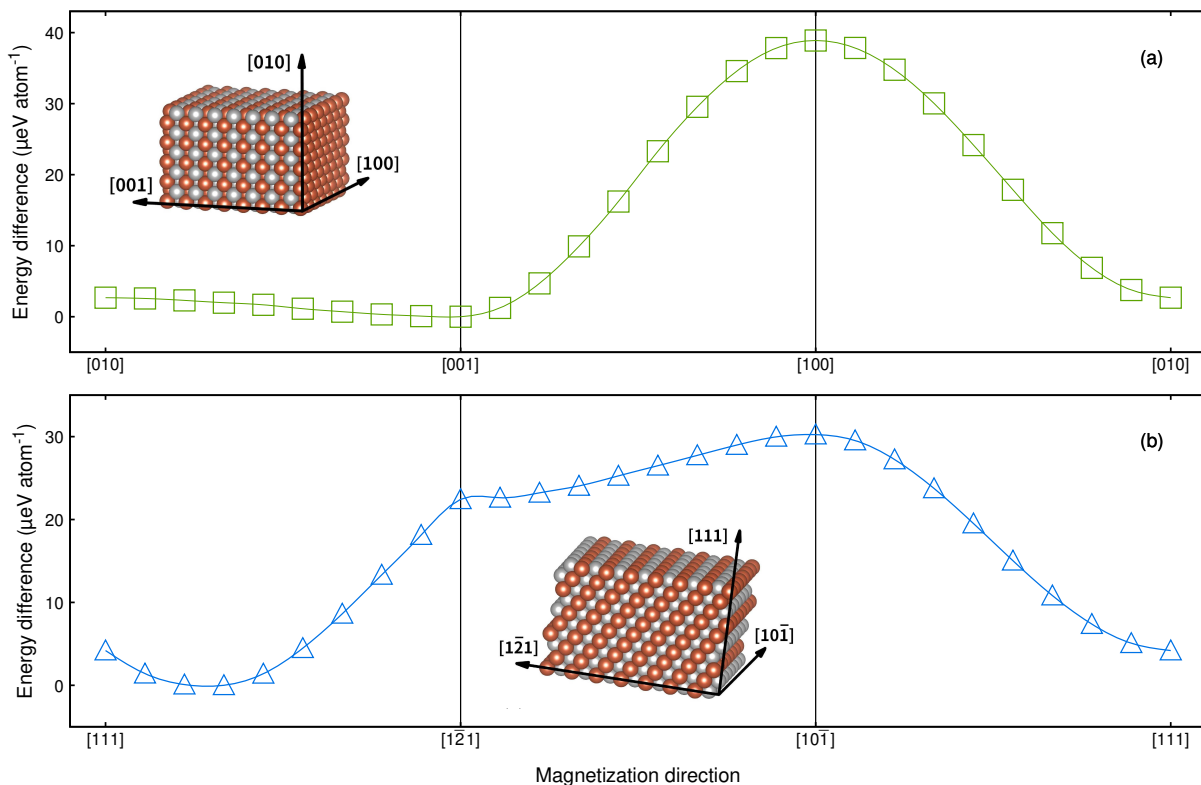


FIG. 8. Evolution of magnetic anisotropy energy with magnetization direction for 10-monolayer films of $L1_0$ FeNi (010) (a) and (111) (b). The calculations were performed using the FPLO18 code with PBE exchange-correlation functional.

is the most energetically stable in this case, see Figs. 6 and 8. Since magnetization has a clear preference in the direction of the tetragonal axis $[001]$, this is not a typical case of in-plane magnetic anisotropy. For distinction, we propose to call it *fixed in-plane* magnetic anisotropy. As in the case of the (001) films discussed above, we also observe oscillations in the magnetic anisotropy energy due to the quantum size effect. Furthermore, as mentioned, bookshelf-type FeNi films with a (110) surface were obtained in 2023 experimentally, but the dependence of the magnetization anisotropy in the plane of the films was not investigated [28]. It is then not clear how shape anisotropy will affect uniaxial anisotropy in this case.

Finally, we will discuss the magnetic anisotropy of (111) films. We do not present for them the dependence of the anisotropy energy on the number of monolayers. Because, as we show, the direction of magnetization changes with film thickness and is tilted to the film surface. For $L1_0$ FeNi (111) films, the angle of the normal to the alternating Fe and Ni monolayers (the tetragonal axis $[001]$) to the out-of-plane direction $[111]$ is 45.615° . This value specifies the axis of easy magnetization within the limits of thick films. For ultrathin films, we expect a deviation of the magnetic easy axis from the tetragonal axis $[001]$. The determined direction of the magnetic easy axis for film (111) with a thickness of 10 atomic monolayers (1.85 nm) is deviated from the $[111]$ direction by 23.8° , see Fig. 8. Figure 7 shows that the direction of the easy axis converges asymptotically to the hypothet-

ical value of 45.615° for the thick (111) films. Whereas, for the thinnest films, the easy axis approaches the out-of-plane direction $[111]$. Although it might be counterintuitive, perhaps it is the ultrathin $L1_0$ FeNi films (111), rather than (001), that will allow for the practical realization of perpendicular magnetic anisotropy? In their favor is the highest energy stability among the three surfaces considered, and the positive results of recent experiments confirming the high values of both the order parameter S and the anisotropy constant K_u (1.15 MJ m^{-3}) [36]. On the other hand, with the uniaxial anisotropy constant tuned in such a way that it only slightly exceeds the shape anisotropy and the direction of the easy axis at 45° to the surface, the $L1_0$ FeNi (111) thin films can become excellent systems for switching devices.

IV. SUMMARY AND CONCLUSIONS

The computational results presented here extend previous research on $L1_0$ FeNi films to include the thinnest films with thickness from 0.5 to 3 nm. Among the films with (001), (010) and (111) surfaces, the latter is the most energetically preferable. Reducing the thickness of ultrathin films raises the magnetic moment by about 5%. In films (001) and (010), the direction of easy magnetization follows the direction of the crystallographic tetragonal axis and is perpendicular to and in the plane of the film, respectively. At the same time, the alignment of the

easy axis in the (010) film plane is unusual in that it is strongly anisotropic in the plane, clearly preferring the direction of the tetragonal axis [001]. For thicker (111) films, the direction of the easy axis of magnetization is consistent with the direction of the tetragonal axis [001] (at the angle of about 45° to the normal to the plane). However, for ultrathin (111) films, it deviates from [001] towards [111] direction (normal to the plane). By this, the magnetic anisotropy of the thinnest (111) films resembles perpendicular anisotropy.

The unique anisotropic properties of $L1_0$ FeNi films may find application in new spintronic devices, as in the case of $L1_0$ FePt films. However, the uniaxial magnetic anisotropy for the $L1_0$ FeNi films is an order of magnitude lower than for the $L1_0$ FePt films and competes with the shape anisotropy. Still, the lower magnetic anisotropy constant may be preferable for some applications, and the

significant price difference between nickel and platinum may also favor FeNi films.

ACKNOWLEDGMENTS

We acknowledge the financial support of the National Science Centre Poland under the decision DEC-2018/30/E/ST3/00267. Part of the computations were performed using resources provided by the Poznan Supercomputing and Networking Center (PSNC). We thank P. Leśniak and D. Depcik for compiling the scientific software and administration of the computing cluster at the Institute of Molecular Physics, Polish Academy of Sciences. We also thank Z. Śniadecki and J. Snarski-Adamski for reading the manuscript and providing valuable comments.

-
- [1] J. Paulevé, D. Dautreppe, J. Laugier, and L. Néel, Une nouvelle transition ordre-désordre dans Fe-Ni (50-50), *J. Phys. Radium* **23**, 841 (1962).
 - [2] L. Néel, J. Pauleve, R. Pauthenet, J. Laugier, and D. Dautreppe, Magnetic Properties of an Iron-Nickel Single Crystal Ordered by Neutron Bombardment, *J. Appl. Phys.* **35**, 873 (1964).
 - [3] J. Paulevé, A. Chamberod, K. Krebs, and A. Bourret, Magnetization Curves of Fe-Ni (50-50) Single Crystals Ordered by Neutron Irradiation with an Applied Magnetic Field, *J. Appl. Phys.* **39**, 989 (1968).
 - [4] J. F. Petersen, M. Aydin, and J. M. Knudsen, Mössbauer spectroscopy of an ordered phase (superstructure) of FeNi in an iron meteorite, *Phys. Lett. A* **62**, 192 (1977).
 - [5] R. S. Clarke and E. R. D. Scott, Tetrataenite - ordered FeNi, a new mineral in meteorites, *Am. Mineral.* **65**, 624 (1980).
 - [6] J. Woolley and B. Bates, Ordering in CoPt-FePt alloys, *J. Common Met.* **1**, 382 (1959).
 - [7] D. E. Laughlin, K. Srinivasan, M. Tanase, and L. Wang, Crystallographic aspects of $L1_0$ magnetic materials, *Scr. Mater.* **53**, 383 (2005).
 - [8] P. Wasilewski, Magnetic characterization of the new magnetic mineral tetrataenite and its contrast with isochemical taenite, *Phys. Earth Planet. Inter.* **52**, 150 (1988).
 - [9] M. Kotsugi, C. Mitsumata, H. Maruyama, T. Wakita, T. Taniuchi, K. Ono, M. Suzuki, N. Kawamura, N. Ishimatsu, M. Oshima, Y. Watanabe, and M. Taniguchi, Novel Magnetic Domain Structure in Iron Meteorite Induced by the Presence of $L1_0$ -FeNi, *Appl. Phys. Express* **3**, 013001 (2010).
 - [10] M. Kotsugi, H. Maruyama, N. Ishimatsu, N. Kawamura, M. Suzuki, M. Mizumaki, K. Osaka, T. Matsumoto, T. Ohkochi, T. Ohtsuki, T. Kojima, M. Mizuguchi, K. Takanashi, and Y. Watanabe, Structural, magnetic and electronic state characterization of $L1_0$ -type ordered FeNi alloy extracted from a natural meteorite, *J. Phys. Condens. Matter* **26**, 064206 (2014).
 - [11] L. H. Lewis, A. Mubarak, E. Poirier, N. Bordeaux, P. Manchanda, A. Kashyap, R. Skomski, J. Goldstein, F. E. Pinkerton, R. K. Mishra, R. C. Kubic Jr, and K. Barmak, Inspired by nature: Investigating tetrataenite for permanent magnet applications, *J. Phys. Condens. Matter* **26**, 064213 (2014).
 - [12] E. Poirier, F. E. Pinkerton, R. Kubic, R. K. Mishra, N. Bordeaux, A. Mubarak, L. H. Lewis, J. I. Goldstein, R. Skomski, and K. Barmak, Intrinsic magnetic properties of $L1_0$ FeNi obtained from meteorite NWA 6259, *J. Appl. Phys.* **117**, 17E318 (2015).
 - [13] T. Shima, M. Okamura, S. Mitani, and K. Takanashi, Structure and magnetic properties for $L1_0$ -ordered FeNi films prepared by alternate monatomic layer deposition, *J. Magn. Magn. Mater.* **310**, 2213 (2007).
 - [14] M. Mizuguchi, S. Sekiya, and K. Takanashi, Characterization of Cu buffer layers for growth of $L1_0$ -FeNi thin films, *J. Appl. Phys.* **107**, 09A716 (2010).
 - [15] T. Kojima, M. Mizuguchi, and K. Takanashi, $L1_0$ -ordered FeNi film grown on Cu-Ni binary buffer layer, *J. Phys. Conf. Ser.* **266**, 012119 (2011).
 - [16] M. Mizuguchi, T. Kojima, M. Kotsugi, T. Koganezawa, K. Osaka, and K. Takanashi, Artificial Fabrication and Order Parameter Estimation of $L1_0$ -ordered FeNi Thin Film Grown on a AuNi Buffer Layer, *J. Magn. Soc. Jpn.* **35**, 370 (2011).
 - [17] T. Kojima, M. Mizuguchi, T. Koganezawa, K. Osaka, M. Kotsugi, and K. Takanashi, Magnetic Anisotropy and Chemical Order of Artificially Synthesized $L1_0$ -Ordered FeNi Films on Au-Cu-Ni Buffer Layers, *Jpn. J. Appl. Phys.* **51**, 010204 (2012).
 - [18] M. Kotsugi, M. Mizuguchi, S. Sekiya, M. Mizumaki, T. Kojima, T. Nakamura, H. Osawa, K. Kodama, T. Ohtsuki, T. Ohkochi, K. Takanashi, and Y. Watanabe, Origin of strong magnetic anisotropy in $L1_0$ -FeNi probed by angular-dependent magnetic circular dichroism, *J. Magn. Magn. Mater.* **326**, 235 (2013).
 - [19] M. Ogiwara, S. Iihama, T. Seki, T. Kojima, S. Mizukami, M. Mizuguchi, and K. Takanashi, Magnetization damping of an $L1_0$ -FeNi thin film with perpendicular magnetic anisotropy, *Appl. Phys. Lett.* **103**, 242409 (2013).
 - [20] T. Ohtsuki, M. Kotsugi, T. Ohkochi, S. Lee, Z. Horita, and K. Takanashi, Nanoscale characterization of FeNi

- alloys processed by high-pressure torsion using photoelectron emission microscope, *J. Appl. Phys.* **114**, 143905 (2013).
- [21] T. Kojima, M. Mizuguchi, T. Koganezawa, M. Ogiwara, M. Kotsugi, T. Ohtsuki, T.-Y. Tashiro, and K. Takanashi, Addition of Co to L1₀-ordered FeNi films: Influences on magnetic properties and ordered structures, *J. Phys. Appl. Phys.* **47**, 425001 (2014).
- [22] K. Mibu, T. Kojima, M. Mizuguchi, and K. Takanashi, Local structure and magnetism of L1₀-type FeNi alloy films with perpendicular magnetic anisotropy studied through ⁵⁷Fe nuclear probes, *J. Phys. Appl. Phys.* **48**, 205002 (2015).
- [23] T. Ueno, K. Saito, N. Inami, T. Kojima, M. Mizuguchi, N. Miyata, K. Akutsu, M. Takeda, K. Takanashi, and K. Ono, Structural and Magnetic Depth Profile Analysis of L1₀ FeNi Film by Polarized Neutron Reflectometry, in *Proc. 2nd Int. Symp. Sci. J-PARC* (Journal of the Physical Society of Japan, Tsukuba, Ibaraki, Japan, 2015).
- [24] T. Kojima, M. Mizuguchi, and K. Takanashi, Growth of L1₀-FeNi thin films on Cu(001) single crystal substrates using oxygen and gold surfactants, *Thin Solid Films* **603**, 348 (2016).
- [25] T. Tashiro, M. Mizuguchi, T. Kojima, T. Koganezawa, M. Kotsugi, T. Ohtsuki, K. Sato, T. Konno, and K. Takanashi, Fabrication of L1₀-FeNi phase by sputtering with rapid thermal annealing, *J. Alloys Compd.* **750**, 164 (2018).
- [26] K. Ito, M. Hayashida, H. Masuda, T. Nishio, S. Goto, H. Kura, T. Koganezawa, M. Mizuguchi, Y. Shimada, T. J. Konno, H. Yanagihara, and K. Takanashi, Epitaxial L1₀-FeNi films with high degree of order and large uniaxial magnetic anisotropy fabricated by denitriding FeNiN films, *Appl. Phys. Lett.* **116**, 242404 (2020).
- [27] T. Nishio, H. Kura, K. Ito, K. Takanashi, and H. Yanagihara, Fabrication of L1₀-FeNi films with island structures by nitrogen insertion and topotactic extraction for improved coercivity, *APL Mater.* **9**, 091108 (2021).
- [28] K. Ito, T. Ichimura, M. Hayashida, T. Nishio, S. Goto, H. Kura, R. Sasaki, M. Tsujikawa, M. Shirai, T. Koganezawa, M. Mizuguchi, Y. Shimada, T. J. Konno, H. Yanagihara, and K. Takanashi, Fabrication of L1₀-ordered FeNi films by denitriding FeNiN(001) and FeNiN(110) films, *J. Alloys Compd.* **946**, 169450 (2023).
- [29] T. Nishio, K. Ito, H. Kura, K. Takanashi, and H. Yanagihara, Uniaxial magnetic anisotropy of L1₀-FeNi films with island structures on LaAlO₃(110) substrates by nitrogen insertion and topotactic extraction, *J. Alloys Compd.* **976**, 172992 (2024).
- [30] K. Takanashi, M. Mizuguchi, T. Kojima, and T. Tashiro, Fabrication and characterization of L1₀-ordered FeNi thin films, *J. Phys. Appl. Phys.* **50**, 483002 (2017).
- [31] Z. Chen, S. Li, and T. Lai, Laser-induced transient strengthening of coupling in L1₀-FePt/FeNi exchange-spring film, *J. Phys. Appl. Phys.* **48**, 145002 (2015).
- [32] A. Svalov, B. González Asensio, A. Chlenova, P. Savin, A. Larrañaga, J. Gonzalez, and G. Kurlyandskaya, Study of the effect of the deposition rate and seed layers on structure and magnetic properties of magnetron sputtered FeNi films, *Vacuum* **119**, 245 (2015).
- [33] A. Frisk, B. Lindgren, S. D. Pappas, E. Johansson, and G. Andersson, Resonant x-ray diffraction revealing chemical disorder in sputtered L1₀ FeNi on Si(0 0 1), *J. Phys.: Condens. Matter* **28**, 406002 (2016).
- [34] A. Frisk, T. P. A. Hase, P. Svedlindh, E. Johansson, and G. Andersson, Strain engineering for controlled growth of thin-film FeNi L1₀, *J. Phys. Appl. Phys.* **50**, 085009 (2017).
- [35] G. Giannopoulos, G. Barucca, A. Kaidatzis, V. Psycharis, R. Salikhov, M. Farle, E. Koutsouflakis, D. Niarchos, A. Mehta, M. Scuderi, G. Nicotra, C. Spinella, S. Laureti, and G. Varvaro, L1₀-FeNi films on Au-Cu-Ni buffer-layer: A high-throughput combinatorial study, *Sci. Rep.* **8**, 15919 (2018).
- [36] V. Q. Nguyen, B.-H. Jun, Y.-B. Chun, and J. H. Lee, Ordered L1₀-FeNi (111) epitaxial thin film on Al₂O₃ (0001) substrate: Molecular beam epitaxy growth and characterizations, *Thin Solid Films* **780**, 139962 (2023).
- [37] S. Mandal, M. Debata, P. Sengupta, and S. Basu, L1₀ FeNi: A promising material for next generation permanent magnets, *Crit. Rev. Solid State Mater. Sci.* **48**, 703 (2023).
- [38] M. Sakamaki and K. Amemiya, Effect of structural strain on magnetic anisotropy energy of each element in alternately layered FeNi thin films, *Phys. Rev. B* **87**, 014428 (2013).
- [39] T. Kojima, M. Ogiwara, M. Mizuguchi, M. Kotsugi, T. Koganezawa, T. Ohtsuki, T.-Y. Tashiro, and K. Takanashi, Fe-Ni composition dependence of magnetic anisotropy in artificially fabricated L1₀-ordered FeNi films, *J. Phys. Condens. Matter* **26**, 064207 (2014).
- [40] L. H. Lewis, F. E. Pinkerton, N. Bordeaux, A. Mubarak, E. Poirier, J. I. Goldstein, R. Skomski, and K. Barmak, De Magnete et Meteorite: Cosmically Motivated Materials, *IEEE Magn. Lett.* **5**, 1 (2014).
- [41] C. W. Yang, D. B. Williams, and J. I. Goldstein, A revision of the Fe-Ni phase diagram at low temperatures (<400 °C), *J. Phase Equilibria* **17**, 522 (1996).
- [42] R. Wu and A. J. Freeman, Spin-orbit induced magnetic phenomena in bulk metals and their surfaces and interfaces, *J. Magn. Magn. Mater.* **200**, 498 (1999).
- [43] P. Ravindran, A. Kjekshus, H. Fjellvåg, P. James, L. Nordström, B. Johansson, and O. Eriksson, Large magnetocrystalline anisotropy in bilayer transition metal phases from first-principles full-potential calculations, *Phys. Rev. B* **63**, 144409 (2001).
- [44] Y. Miura, S. Ozaki, Y. Kuwahara, M. Tsujikawa, K. Abe, and M. Shirai, The origin of perpendicular magneto-crystalline anisotropy in L1₀ FeNi under tetragonal distortion, *J. Phys. Condens. Matter* **25**, 106005 (2013).
- [45] A. Edström, J. Chico, A. Jakobsson, A. Bergman, and J. Ruzs, Electronic structure and magnetic properties of L1₀ binary alloys, *Phys. Rev. B* **90**, 014402 (2014).
- [46] P. Manchanda, R. Skomski, N. Bordeaux, L. H. Lewis, and A. Kashyap, Transition-metal and metalloid substitutions in L1₀-ordered FeNi, *J. Appl. Phys.* **115**, 17A710 (2014).
- [47] M. Werwiński and W. Marciniak, Ab initio study of magnetocrystalline anisotropy, magnetostriction, and Fermi surface of L1₀ FeNi (tetrataenite), *J. Phys. Appl. Phys.* **50**, 495008 (2017).
- [48] L.-Y. Tian, H. Levämäki, O. Eriksson, K. Kokko, Á. Nagy, E. K. Délczeg-Czirják, and L. Vitos, Density Functional Theory description of the order-disorder transformation in Fe-Ni, *Sci. Rep.* **9**, 8172 (2019).
- [49] L.-Y. Tian, O. Eriksson, and L. Vitos, Pressure effect on the order-disorder transformation in L1₀ FeNi, *Sci.*

- Rep. **10**, 14766 (2020).
- [50] L.-Y. Tian, O. Gutfleisch, O. Eriksson, and L. Vitos, Alloying effect on the order–disorder transformation in tetragonal FeNi, *Sci. Rep.* **11**, 5253 (2021).
- [51] D. Tuvshin, T. Tsevelmaa, S. Hong, and D. Odkhuu, Fe-Ni-N based alloys as rare-earth free high-performance permanent magnet across α'' to L1₀ phase transition: A theoretical insight, *Acta Mater.* **210**, 116807 (2021).
- [52] M. Si, A. Izardar, and C. Ederer, Effect of chemical disorder on the magnetic anisotropy in L1₀ FeNi from first-principles calculations, *Phys. Rev. Res.* **4**, 033161 (2022).
- [53] Z. Qiao, M. Tsujikawa, and M. Shirai, The effect of chemical disorder on magnetic properties of FeNi and Fe₂Ni₂N alloys, *J. Magn. Magn. Mater.* **568**, 170362 (2023).
- [54] C. D. Woodgate, C. E. Patrick, L. H. Lewis, and J. B. Staunton, Revisiting Néel 60 years on: The magnetic anisotropy of L1₀ FeNi (tetrataenite), *J. Appl. Phys.* **134**, 163905 (2023).
- [55] S. Yamashita and A. Sakuma, Finite-temperature second-order perturbation analysis of magnetocrystalline anisotropy energy of L1₀-type ordered alloys, *Phys. Rev. B* **108**, 054411 (2023).
- [56] S. Simonetti, G. Brizuela, and A. Juan, Study of the adsorption, electronic structure and bonding of C₂H₄ on the FeNi(111) surface, *Appl. Surf. Sci.* **256**, 6459 (2010).
- [57] Y.-B. He, J.-F. Jia, and H.-S. Wu, First-Principles Investigation of the Molecular Adsorption and Dissociation of Hydrazine on Ni–Fe Alloy Surfaces, *J. Phys. Chem. C* **119**, 8763 (2015).
- [58] H. Zhang, M. Richter, K. Koepf, I. Opahle, F. Tasnádi, and H. Eschrig, Electric-field control of surface magnetic anisotropy: A density functional approach, *New J. Phys.* **11**, 043007 (2009).
- [59] G. Géranton, F. Freimuth, S. Blügel, and Y. Mokrousov, Spin-orbit torques in L1₀-FePt/Pt thin films driven by electrical and thermal currents, *Phys. Rev. B* **91**, 014417 (2015).
- [60] Z. Liu, Y. Lei, and G. Wang, First-principles computation of surface segregation in L1₀ CoPt magnetic nanoparticles, *J. Phys. Condens. Matter* **28**, 266002 (2016).
- [61] S. Mao, J. Lu, X. Zhao, X. Wang, D. Wei, J. Liu, J. Xia, and J. Zhao, MnGa-based fully perpendicular magnetic tunnel junctions with ultrathin Co₂MnSi interlayers, *Sci. Rep.* **7**, 43064 (2017).
- [62] A. Tellez-Mora, H. Fernandez-Escamilla, R. Ponce-Perez, N. Takeuchi, and J. Guerrero-Sanchez, Controlling the magnetic alignment at the MnGa/Co₂MnSi interface: A DFT study, *J. Magn. Magn. Mater.* **547**, 168936 (2022).
- [63] J. Marciniak and M. Werwiński, L1₀ FePt thin films with tilted and in-plane magnetic anisotropy: A first-principles study, *Phys. Rev. B* **108**, 214406 (2023).
- [64] J. Marciniak, W. Marciniak, and M. Werwiński, DFT calculation of intrinsic properties of magnetically hard phase L1₀ FePt, *J. Magn. Magn. Mater.* **556**, 169347 (2022).
- [65] G. Varvaro, P. Imperatori, S. Laureti, D. Peddis, F. Locardi, M. Ferretti, C. Cannas, M. S. Angotzi, N. Yacoub, and A. Capobianchi, Facile and fast synthesis of highly ordered L1₀-FeNi nanoparticles, *Scr. Mater.* **238**, 115754 (2024).
- [66] J. Wang, Y. Hirayama, K. Suzuki, K. Park, Z. Liu, K. Takagi, and K. Ozaki, Nanotwin-assisted nitridation of quenched FeNi alloy nanopowders for rare-earth-free magnets, *J. Mater. Sci. Technol.* **165**, 244 (2023).
- [67] J. Liang, Z. Zhao, N. Li, X. Wang, S. Li, X. Liu, T. Wang, G. Lu, D. Wang, B.-J. Hwang, Y. Huang, D. Su, and Q. Li, Biaxial Strains Mediated Oxygen Reduction Electrocatalysis on Fenton Reaction Resistant L1₀-PtZn Fuel Cell Cathode, *Adv. Energy Mater.* **10**, 2000179 (2020).
- [68] J. Liang, N. Li, Z. Zhao, L. Ma, X. Wang, S. Li, X. Liu, T. Wang, Y. Du, G. Lu, J. Han, Y. Huang, D. Su, and Q. Li, Tungsten-Doped L1₀-PtCo Ultrasmall Nanoparticles as a High-Performance Fuel Cell Cathode, *Angew. Chem. Int. Ed.* **58**, 15471 (2019).
- [69] T. Wang, J. Liang, Z. Zhao, S. Li, G. Lu, Z. Xia, C. Wang, J. Luo, J. Han, C. Ma, Y. Huang, and Q. Li, Sub-6 nm Fully Ordered L1₀-Pt–Ni–Co Nanoparticles Enhance Oxygen Reduction via Co Doping Induced Ferromagnetism Enhancement and Optimized Surface Strain, *Adv. Energy Mater.* **9**, 1803771 (2019).
- [70] A. Kovacs, H. Ozelt, J. Fischbacher, T. Schrefl, A. Kaidatzis, R. Salikhov, M. Farle, G. Giannopoulos, and D. Niarchos, Micromagnetic Simulations for Coercivity Improvement through Nano-Structuring of Rare-Earth Free L1₀-FeNi Magnets, *IEEE Trans. Magn.* **53**, 1 (2017).
- [71] J. Fischbacher, A. Kovacs, M. Gusenbauer, H. Ozelt, L. Exl, S. Bance, and T. Schrefl, Micromagnetics of rare-earth efficient permanent magnets, *J. Phys. Appl. Phys.* **51**, 193002 (2018).
- [72] S. Goto, H. Kura, E. Watanabe, Y. Hayashi, H. Yanagihara, Y. Shimada, M. Mizuguchi, K. Takanashi, and E. Kita, Synthesis of single-phase L1₀-FeNi magnet powder by nitrogen insertion and topotactic extraction, *Sci. Rep.* **7**, 13216 (2017).
- [73] Y. P. Ivanov, B. Sarac, S. V. Ketov, J. Eckert, and A. L. Greer, Direct Formation of Hard-Magnetic Tetrataenite in Bulk Alloy Castings, *Adv. Sci.* **10**, 2204315 (2023).
- [74] L. H. Lewis and P. S. Stamenov, Accelerating Nature: Induced Atomic Order in Equiatomic FeNi, *Adv. Sci.* **10**, 2302696 (2023).
- [75] R. McCallum, L. Lewis, R. Skomski, M. Kramer, and I. Anderson, Practical Aspects of Modern and Future Permanent Magnets, *Annu. Rev. Mater. Res.* **44**, 451 (2014).
- [76] S. Hirotsawa, Current Status of Research and Development toward Permanent Magnets Free from Critical Elements, *J. Magn. Soc. Jpn.* **3**, 85 (2015).
- [77] R. Skomski and J. Coey, Magnetic anisotropy — How much is enough for a permanent magnet?, *Scr. Mater.* **112**, 3 (2016).
- [78] M. Albrecht, G. Hu, I. L. Guhr, T. C. Ulbrich, J. Boneberg, P. Leiderer, and G. Schatz, Magnetic multilayers on nanospheres, *Nat. Mater.* **4**, 203 (2005).
- [79] J.-P. Wang, Tilting for the top, *Nat. Mater.* **4**, 191 (2005).
- [80] C. L. Zha, J. Persson, S. Bonetti, Y. Y. Fang, and J. Åkerman, Pseudo spin valves based on L1₀ (111)-oriented FePt fixed layers with tilted anisotropy, *Appl. Phys. Lett.* **94**, 163108 (2009).
- [81] Y.-N. Hsu, S. Jeong, D. Lambeth, and D. Laughlin, In situ ordering of FePt thin films by using Ag/Si and Ag/Mn₃Si/Ag/Si templates, *IEEE Trans. Magn.* **36**, 2945 (2000).
- [82] T. Shima, K. Takanashi, Y. K. Takahashi, and K. Hono,

- Preparation and magnetic properties of highly coercive FePt films, *Appl. Phys. Lett.* **81**, 1050 (2002).
- [83] M. Ohtake, S. Ouchi, F. Kirino, and M. Futamoto, L10 ordered phase formation in FePt, FePd, CoPt, and CoPd alloy thin films epitaxially grown on MgO(001) single-crystal substrates, *J. Appl. Phys.* **111**, 07A708 (2012).
- [84] H. Sepehri-Amin, H. Iwama, T. Ohkubo, T. Shima, and K. Hono, Microstructure and in-plane component of L1₀-FePt films deposited on MgO and MgAl₂O₄ substrates, *Scr. Mater.* **130**, 247 (2017).
- [85] K. Wu, X. Fu, W. Zhu, and X. Huang, Atomic-scale investigation on the origin of in-plane variants in L1₀-FePt nanoparticles embedded in a single-crystalline MgO matrix, *J. Appl. Phys.* **132**, 175305 (2022).
- [86] K. Koepnik and H. Eschrig, Full-potential nonorthogonal local-orbital minimum-basis band-structure scheme, *Phys. Rev. B* **59**, 1743 (1999).
- [87] I. Opahle, K. Koepnik, and H. Eschrig, Full-potential band-structure calculation of iron pyrite, *Phys. Rev. B* **60**, 14035 (1999).
- [88] J. P. Perdew, K. Burke, and M. Ernzerhof, Generalized gradient approximation made simple, *Phys. Rev. Lett.* **77**, 3865 (1996).
- [89] W. Marciniak and M. Werwiński, Structural and magnetic properties of Fe-Co-C alloys with tetragonal deformation: A first-principles study, *Phys. Rev. B* **108**, 214433 (2023).
- [90] J. P. Perdew and Y. Wang, Accurate and simple analytic representation of the electron-gas correlation energy, *Phys. Rev. B* **45**, 13244 (1992).
- [91] R. S. Mulliken, Electronic Population Analysis on LCAO-MO Molecular Wave Functions. I, *J. Chem. Phys.* **23**, 1833 (1955).
- [92] K. Momma and F. Izumi, *VESTA*: A three-dimensional visualization system for electronic and structural analysis, *J. Appl. Crystallogr.* **41**, 653 (2008).
- [93] Z. Li, K. Zhang, L. Shen, X. Xie, W. Chen, Z. Zhou, L. Lu, M. Liu, S. Yan, W. Zhao, and Q. Leng, Field-Free Magnetization Switching Induced by Bulk Spin-Orbit Torque in a (111)-Oriented CoPt Single Layer with In-Plane Remanent Magnetization, *ACS Appl. Electron. Mater.* **4**, 4033 (2022).
- [94] A. Dannenberg, M. E. Gruner, A. Hucht, and P. Entel, Surface energies of stoichiometric FePt and CoPt alloys and their implications for nanoparticle morphologies, *Phys. Rev. B* **80**, 245438 (2009).
- [95] J. I. Beltrán, L. Balcells, and C. Martínez-Boubeta, Interfacial geometry dependence of the iron magnetic moment: The case of MgO/Fe/MgO, *Phys. Rev. B* **85**, 064417 (2012).
- [96] L. Szunyogh, B. Újfalussy, C. Blaas, U. Pustogowa, C. Sommers, and P. Weinberger, Oscillatory behavior of the magnetic anisotropy energy in Cu(100)/Co_n multilayer systems, *Phys. Rev. B* **56**, 14036 (1997).
- [97] M. Blanco-Rey, P. Perna, A. Gudin, J. M. Diez, A. Anadón, P. Olleros-Rodríguez, L. De Melo Costa, M. Valvidares, P. Gargiani, A. Guedeja-Marron, M. Cabero, M. Varela, C. García-Fernández, M. M. Otrokov, J. Camarero, R. Miranda, A. Arnau, and J. I. Cerdá, Large Perpendicular Magnetic Anisotropy in Nanometer-Thick Epitaxial Graphene/Co/Heavy Metal Heterostructures for Spin-Orbitronics Devices, *ACS Appl. Nano Mater.* **4**, 4398 (2021).
- [98] P.-H. Chang, W. Fang, T. Ozaki, and K. D. Belashchenko, Voltage-controlled magnetic anisotropy in antiferromagnetic MgO-capped MnPt films, *Phys. Rev. Mater.* **5**, 054406 (2021).
- [99] M. Cinal, Magnetic anisotropy and orbital magnetic moment in Co films and Co/X bilayers (X = Pd and Pt), *Phys. Rev. B* **105**, 104403 (2022).
- [100] M. Przybylski, M. Dąbrowski, U. Bauer, M. Cinal, and J. Kirschner, Oscillatory magnetic anisotropy due to quantum well states in thin ferromagnetic films (invited), *J. Appl. Phys.* **111**, 07C102 (2012).